Solar-Terrestrial Physics. 2025, vol. 11, iss.2, pp. 119–124. DOI: 10.12737/stp-112202512. © 2025
P.A. Kruchinin, S.A. Siruk, A.G. Mayorov, V.V. Malakhov, S.Yu. Aleksandrin. Published by INFRA-M Academic Publishing House

DOI: 10.12737/stp-112202512

Received March 29, 2025
Accepted May 12, 2025

GEOMAGNETIC CUTOFF RIGIDITY IN NEUTRON MONITOR LOCATIONS

P.A. Kruchinin
National Research Nuclear University MEPhI, Moscow, Russia, kruchinin_01@inbox.ru

S.A. Siruk
National Research Nuclear University MEPhI, Moscow, Russia, sstepana001@mail.ru

A.G. Mayorov
National Research Nuclear University MEPhI, Moscow, Russia, agmayorov@mephi.ru

V.V. Malakhov
National Research Nuclear University MEPhI, Moscow, Russia, vvmalakhov@mephi.ru

S.Yu. Aleksandrin
National Research Nuclear University MEPhI, Moscow, Russia, SYaleksandrin@mephi.ru

Abstract. Neutron monitors (NMs), located at different points on the planet, allow us to study the time, energy, and angular characteristics of galactic and solar particle fluxes. Since NMs are located inside Earth's magnetosphere, their response depends on their location on the planet's surface, which can be characterized by the geomagnetic cutoff rigidity. Its calculation depends on the magnetic field model, the date, and even on numerical methods. The paper presents calculated geomagnetic cutoff rigidities at the locations of some neutron monitors and compares the cutoff values with the calculation results obtained by other authors, including a comparison of the time dynamics over the past decade. We show that the geomagnetic cutoff rigidities obtained for 2020 by the IGRF-14 model differ from those derived by IGRF-13; however, for 2015 the difference between the models is negligible. We demonstrate a tendency for the geomagnetic cutoff rigidity to decrease over time, especially at midlatitudes. Comparison of the obtained geomagnetic cutoff rigidities with those obtained by other authors has shown that in most cases the difference does not exceed 0.2 GV. Such discrepancies are significant only in the circumpolar region, where particles are mostly shielded by Earth's atmosphere rather than by the geomagnetic field. We show that the accuracy of the algorithm in use is comparable to that of other existing instruments and is sufficient for calculating neutron monitor responses.

Keywords: geomagnetic field, geomagnetic cutoff rigidity, cosmic rays, neutron monitors.

INTRODUCTION

The geomagnetic cutoff rigidity $R_c(\varphi, \lambda, h, \Theta, \Psi)$ is the minimum magnetic rigidity (particle momentum divided by its charge) that a particle must possess in order to reach a given point in near-Earth space (set by latitude φ, longitude λ, and height h) while moving from a certain direction (characterized by the zenith angle Θ and the azimuth angle Ψ) [Cooke et al., 1991]. In practice, the so-called effective vertical cutoff rigidity R_{eff} is most often used which is calculated for particles coming from the vertical direction, taking into account the penumbra region of geomagnetic cutoff.

Knowledge of R_c is important for many applied and fundamental problems of geophysics and cosmic ray (CR) physics, such as assessing the radiation level [Tezari et al., 2020], examining the dynamics of the geomagnetic field and CR variations on large time scales [Gvozdevsky et al., 2018], studying geomagnetic storms [Tyasto et al. al., 2013], and simulating the response of cosmic-ray detectors [Mishev et al., 2020]. The accuracy of R_c reconstruction is especially important in working with neutron monitors (NMs) located in the range R_{eff}~1 GV, where the CR geomagnetic cutoff competes with the atmospheric cutoff [Poluianov, Batalla, 2022].

In addition to the fact that R_c changes with time, the values for the same period presented in various works [Smart, Shea, 2019; Abunina et al., 2020; Mishev et al., 2020; Gerontidou et al., 2021; Poluianov, Batalla, 2022] also differ. In this paper, we calculate effective vertical R_c at locations of several NMs in 2015–2025, examine its temporal dynamics, and compare it with those obtained in other studies.

1. METHOD

The main method of calculating R_c is to solve equations of charged particle motion in various magnetic field models. We employ the GetTrajectory (GT) software package [https://github.com/agmayorov/GTsimulation]. The software package includes a tracing algorithm based on the particle-in-cell method implemented in the Buneman–Boris scheme [Boris, 1970, 1971]. The method allows us to solve the equations of charged particles moving in a magnetic field while preserving kinetic energy during sustained motion in complex magnetic field, in particular in Earth's magnetic field. Thus, this method proves to be more accurate and stable than the Runge–Kutta method, and faster than other energy-conserving schemes [Mao, Wirz, 2011; Qin et al., 2013]. Calculations have been made for protons at space points corresponding to the geographic coordinates of neutron monitors (Figure 1). Since particles entering the atmosphere at angles other than 90° have to pass through a larger

amount of matter, vertically incident particles contribute decisively to the counting rate of neutron monitors. In this regard, particle backtracing (reconstruction of the trajectory in the opposite direction in time) was carried out at an altitude of 20 km for the vertical direction of arrival.

To calculate R_c at a given space point for the selected arrival direction, a particle was backtraced in the magnetic field until one of the following conditions was met:

1) the particle reached Earth's surface (albedo trajectory);

2) the particle reached a distance equal to 30 Earth radii (galactic trajectory);

3) the lifetime of the particle from the start of tracing was as long as 20 s, but none of the previous conditions held.

The first and third types include particles with forbidden trajectories; the second type, particles with rigidity corresponding to the allowed trajectory [Cooke et al., 1991].

In this work, we have used a magnetic field set by empirical geomagnetic field models IGRF-13 [Alken et al., 2021] and IGRF-14 [https://www.ncei.noaa.gov/products/international-geomagnetic-reference-field].

The geomagnetic field has no clear boundary between allowed and forbidden geomagnetic cutoff rigidities. The region called penumbra is a range with a chaotic set of allowed and forbidden rigidities [Cooke et al., 1991]; therefore, to calculate in the region of the assumed penumbra, we backtraced particles at increments of 0.01 GV for midlatitudes and 0.001 GV for polar regions. The final R_c value was R_{eff} given by the formula [Tyasto et al., 2013]

$R_{eff} = R_u - n_{allowed}\,\Delta R$, where R_u is the upper boundary of the penumbra; $n_{allowed}$ is the number of allowed bands between the upper and lower boundaries of the penumbra; ΔR is the rigidity increment at which the penumbra pattern of geomagnetic cutoff is reconstructed.

2. GEOMAGNETIC CUTOFF RIGIDITY VALUES

Effective R_c R_{eff} is one of the main parameters for simulating the response of neutron monitors. The results presented in Tables 1–3 are for 2025, 2020, and 2015. The calculated values of R_{eff} are intended to be used as reference data.

2.1. 2025

The magnetic field model IGRF-14 has been employed to calculate the geomagnetic cutoff rigidity. The data is presented in Table 1. The results obtained are compared with R_{eff} calculated using the IZMIRAN tool "Cutoff 2050" [https://tools.izmiran.ru/cutoff/].

The deviation of the calculated R_{eff} values from those obtained with the IZMIRAN tool depending on the geomagnetic latitude (Figure 2) suggests that the difference is the greatest in polar regions and minimum at middle and low latitudes. High latitudes correspond to a high magnetic field gradient, and R_c takes on rather low values (<0.1 GV). The eight-fold deviation in this region may be due to differences in particle tracing algorithms.

2.2. 2020

In [Gerontidou et al., 2021; Smart, Shea, 2019], the results are presented as a world grid of R_{eff}. The grid was reconstructed with a certain step in latitude and longitude, so the values of R_{eff} for coordinates of neutron monitors were obtained through third-degree polynomial interpolation. The calculation results are presented in Tables 2 and 3.

Analysis of Figure 3 shows that the largest deviation occurs when we compare our results with calculations by the IZMIRAN tool for polar regions, yet the absolute difference does not exceed 0.1 GV. The greatest agreement is achieved with the results of [Gerontidou et al., 2021] — the relative deviation does not exceed 0.1. In Figure 3 is also a comparison with the values calculated using the developed algorithm, but in IGRF-13. Note that the updated version of the main field IGRF-14 makes a minor contribution to the change in R_c values. This is especially noticeable for midlatitudes (40°–50°).

2.3. 2015

Table 3, similar to Tables 1 and 2, lists R_c given in [Smart, Shea, 2019; Mishev et al., 2020; Abunina et al., 2020].

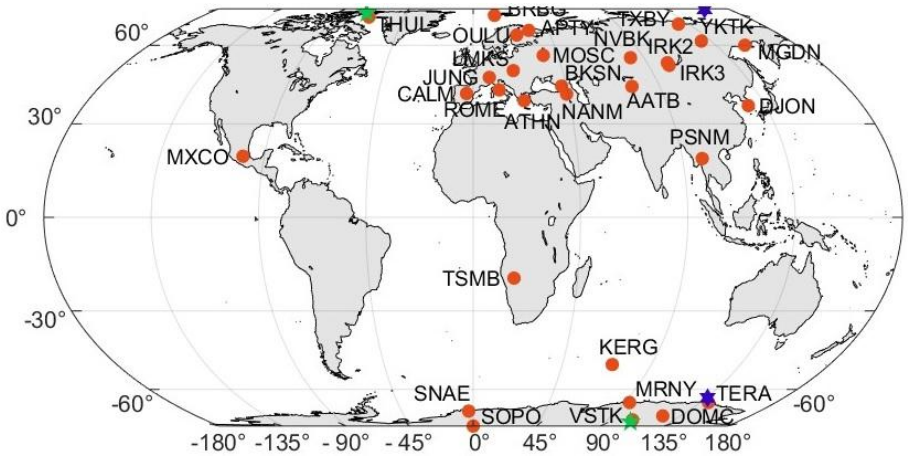

Figure 1. Geographic location of the neutron monitors under study; five-pointed and six-pointed stars indicate geomagnetic and magnetic poles in 2020 respectively.

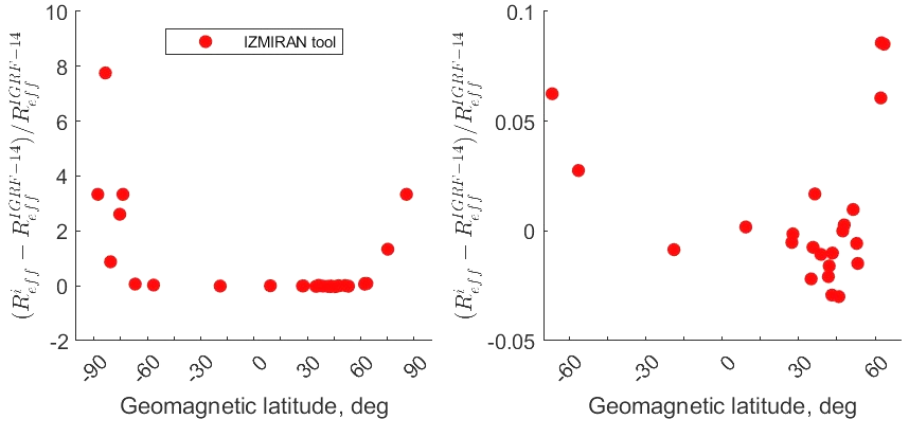

Figure 2. Comparison between the R_c values we have obtained with the values calculated using the IZMIRAN tool for 2025 in the entire range of geomagnetic latitudes (*a*) and without circumpolar regions (*b*)

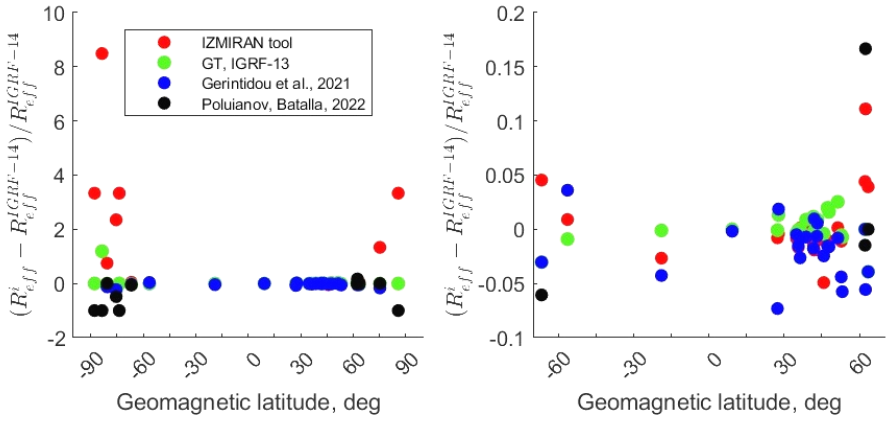

Figure 3. Comparison between R_c for 2020 in the entire range of geomagnetic latitudes (*a*) and without circumpolar regions (*b*)

Table 1

Geomagnetic cutoff rigidities in 2025 calculated for stations' coordinates and altitude

Station code	Station name	Latitude, deg.	Longitude, deg.	Altitude, m	Geomagnetic latitude, deg.	R_{eff}, GV	
						GT, IGRF-14	IZMIRAN tool, IGRF
AATB	Alma-Ata B	43.14	76.6	3340	34.88	5.95	5.82
APTY	Apatity	67.57	33.4	181	63.49	0.47	0.51
ATHN	Athens	37.97	23.78	260	36.34	8.31	8.45
BKSN	Baksan	43.28	42.69	1700	38.71	5.61	5.55
BRBG	Barentsburg	78.06	14.22	70	75.28	0.06	0.14
CALM	Castilla-La Mancha	40.56	–3.16	708	43.24	6.95	6.88
DJON	Daejon	36.24	127.22	200	27.31	11.45	11.39
DOMC	Dome C	–75.10	123.33	3233	–83.56	0.01	0.12
IRK2	Irkutsk2	52.37	100.55	2000	43.02	3.08	2.99
IRK3	Irkutsk3	51.29	100.55	3000	41.65	3.36	3.29
JUNG	Jungfraujoch IGY	46.55	7.98	3570	47.27	4.52	4.52
KERG	Kerguelen	–49.35	70.25	33	–56.45	1.09	1.12
LMKS	Lomnický štít	49.20	20.22	2634	47.86	3.65	3.66
MGDN	Magadan	60.04	151.05	220	52.75	1.76	1.75
MOSC	Moscow	55.47	37.32	200	51.37	2.05	2.07
MRNY	Mirny	–66.55	93.02	30	–75.45	0.04	0.14
MXCO	Mexico	19.33	–99.18	2274	27.73	7.40	7.39
NANM	Nor-Amberd Neutron Monitor	40.37	44.25	2000	35.63	6.69	6.64
NVBK	Novosibirsk	54.48	83	163	45.77	2.34	2.27
OULU	Oulu Neutron Monitor	65.05	25.47	15	62.24	0.66	0.70

PSNM	Princess Sirindhorn Neutron Monitor	18.59	98.49	2565	9.23	16.70	16.73
ROME	Rome	41.86	12.47	0	41.97	6.25	6.15
SNAE	Sanae 6NM64	–71.67	–2.85	856	–66.78	0.64	0.68
SOPO	South Pole	–90.0	0	2820	–80.65	0.08	0.15
TERA	Terre Adelie	–66.55	140	32	–73.68	0.03	0.13
THUL	Thule	76.5	–68.7	26	85.78	0.03	0.13
TSMB	Tsumeb	–19.2	17.58	1240	–18.98	9.38	9.30
TXBY	Tixie Bay	71.36	128.54	0	62.43	0.35	0.38
VSTK	Vostok	–78.47	106.87	3488	–87.82	0.03	0.13
YKTK	Yakutsk	62.01	129.43	105	53.16	1.35	1.33

Table 2

Geomagnetic cutoff rigidity in 2020

Station code	R_{eff}, GV				
	GT, IGRF-13	GT, IGRF-14	IZMIRAN tool, IGRF	Gerontidou et al., 2021	Poluianov, Batalla, 2022
AATB	5.96	5.98	5.93	5.95	–
APTY	0.49	0.51	0.53	0.49	0.51
ATHN	8.36	8.36	8.37	8.14	–
BKSN	5.65	5.60	5.60	5.56	–
BRBG	0.06	0.06	0.14	0.05	0.06
CALM	6.97	6.91	6.84	6.95	–
DJON	11.48	11.49	11.40	10.65	–
DOMC	0.03	0.01	0.13	0.00	0.00
IRK2	3.09	3.07	3.05	3.05	–
IRK3	3.46	3.42	3.37	3.36	–
JUNG	4.62	4.53	4.48	4.46	–
KERG	1.10	1.11	1.12	1.15	–
LMKS	3.78	3.72	3.68	3.66	–
MGDN	1.81	1.82	1.80	1.74	–
MOSC	2.15	2.10	2.10	2.08	–
MRNY	0.03	0.04	0.13	0.03	0.02
MXCO	7.60	7.50	7.47	7.64	–
NANM	6.83	6.83	6.72	6.73	–
NVBK	2,43	2.44	2.32	2.38	–
OULU	0.68	0.68	0.71	0.68	0.67
PSNM	16.72	16.72	16.73	16.69	–
ROME	6.25	6.26	6.14	6.32	–
SNAE	0.64	0.66	0.69	0.64	0.62
SOPO	0.08	0.08	0.14	0.07	0.08
TERA	0.03	0.03	0.13	0.00	0.00
THUL	0.03	0.03	0.13	0.00	0.00
TSMB	9.37	9.38	9.13	8.98	–
TXBY	0.36	0.36	0.40	0.34	0.42
VSTK	0.03	0.03	0.13	0.00	0.00
YKTK	1.38	1.39	1.38	1.31	–

Figure 4 indicates that the largest differences (8–9 times) are observed when we compare the results of our calculations with the results of the IZMIRAN tool and [Mishev et al., 2020] for polar regions. Nonetheless, at middle and low latitudes there is a close fit (0–0.1) between R_c values from all sources considered. The comparison between the IGRF-13 and IGRF-14 results is not shown in Table 3 and the plot since the R_{eff} values for 2015 are the same.

2.4. Temporal dynamics of cutoff rigidity

Annual and secular variations in Earth's magnetosphere cause R_c to change. Figure 5 depicts the absolute difference between R_{eff} values in 2025 and 2015. Analysis of the results confirms the general trend toward a decrease in R_c noted in [Gvozdevsky et al., 2018; Gerontidou et al., 2021]. The maximum decrease (by 0.19 GV) and increase (by 0.07 GV) in R_c correspond to mid-latitudes (40°–50°) of the Northern Hemisphere. The behavior of R_c may be associated with a decrease in the dipole geomagnetic field component and an increase in the nondipole one [Gvozdevsky et al., 2018; Smart, Shea, 2019].

CONCLUSION

The paper reports the calculation results of the geomagnetic cutoff rigidity for a network of neutron monitors, obtained by IGRF-14 for 2015, 2020, and 2025.

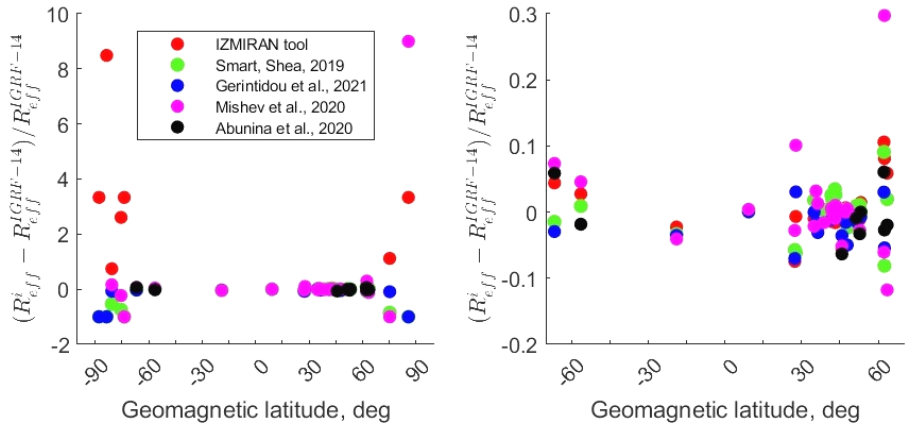

Figure 4. Comparison between R_c values for 2015 in the entire range of geomagnetic latitudes (*a*) and without circumpolar regions (*b*)

Table 3

Geomagnetic cutoff rigidity in 2015

Station code	R_{eff}, GV					
	GT, IGRF-14	IZMIRAN tool, IGRF	Gerontidou et al., 2021	Smart, Shea, 2019	Mishev et al., 2020	Abunina et al., 2020
AATB	6.08	6.02	6.08	6.19	5.95	–
APTY	0.51	0.54	0.50	0.52	0.45	0.50
ATHN	8.42	8.42	8.16	8.28	8.53	–
BKSN	5.69	5.63	5.60	5.71	5.60	–
BRBG	0.07	0.14	0.06	0.01	0.00	–
CALM	6.88	6.77	6.88	7.06	6.95	–
DJON	11.54	10.68	10.73	10.88	11.22	–
DOMC	0.01	0.13	0.00	0.00	–	–
IRK2	3.16	3.12	3.14	3.27	3.13	–
IRK3	3.49	3.44	3.45	3.58	3.51	–
JUNG	4.49	4.52	4.42	4.51	4.49	–
KERG	1.09	1.12	1.14	1.10	1.14	1.07
LMKS	3.82	3.73	3.63	3.73	3.84	–
MGDN	1.83	1.81	1.78	1.85	1.78	1.77
MOSC	2.14	2.14	2.11	2.16	2.13	2.12
MRNY	0.04	0.14	0.03	0.01	0.03	–
MXCO	7.52	7.47	7.75	7.06	8.28	–
NANM	6.88	6.84	6.77	6.89	7.10	–
NVBK	2.53	2.39	2.44	2.53	2.40	2.37
OULU	0.66	0.73	0.68	0.72	0.62	0.70
PSNM	16.73	16.74	16.74	16.74	16.8	–
ROME	6.27	6.23	6.30	6.39	6.27	–
SNAE	0.68	0.71	0.66	0.67	0.73	0.72
SOPO	0.09	0.15	0.08	0.04	0.10	–
TERA	0.03	0.13	0.00	0.00	0.00	–
THUL	0.03	0.13	0.00	0.00	0.30	–
TSMB	9.33	9.12	9.00	9.02	8.95	–
TXBY	0.37	0.40	0.35	0.34	0.48	0.36
VSTK	0.03	0.13	0.00	0.00	–	–
YKTK	1.37	1.39	1.36	1.37	1.37	1.37

The calculation was carried out using the GT software package, which employs the particle tracing algorithm under the particle-in-cell scheme implemented by the Buneman–Boris method. We have compared the results with the data acquired by the IZMIRAN tool, as well as those presented by different authors. There is a good fit (relative deviation no more than 10 %) between different calculations at low and middle latitudes, and the absolute difference for most neutron monitors does not exceed 0.2 GV. Such deviations resulting from different tracing methods are significant in the circumpolar region, where atmospheric shielding plays an important role. Thus, the accuracy of the algorithm in use is sufficient for correct work with ground-based CR detectors.

Comparison of geomagnetic cutoff rigidities in 2015 and 2025 has shown that R_{eff} increases for some neutron

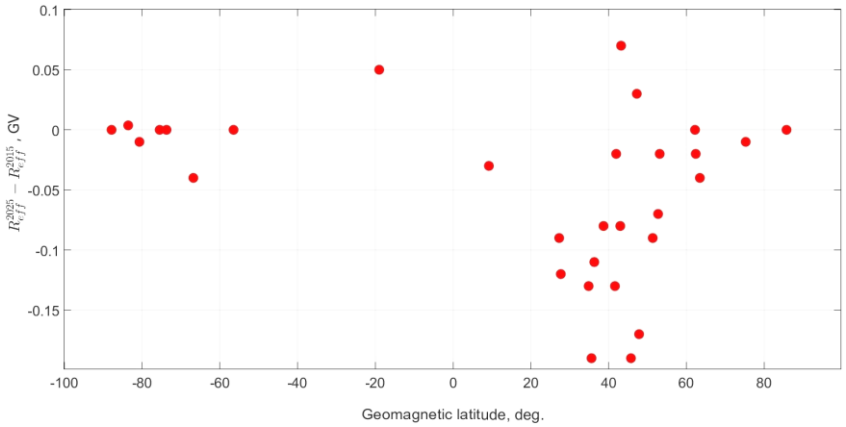

Figure 5. Change in the effective geomagnetic cutoff rigidity for neutron monitors in 2025 compared to 2015

monitor stations at midlatitudes of the Northern Hemisphere (for example, 0.07 GV for CALM in Spain). This can be explained by the fact that the location of the scientific stations corresponds to the periphery of the North Atlantic Anomaly, where R_c increases. However, at most CR stations with neutron monitors R_c decreases with a maximum decrease of 0.19 GV in the Northern Hemisphere at geomagnetic latitudes 40°–50°.

Since many works still employ the old R_c values calculated for 1965, we recommend using the R_c data presented in this work for 2015–2025 in order to obtain more reliable results when studying the observable CR effects.

The geomagnetic coordinates were obtained from the British Geological Survey — Geomagnetism service [https://geom ag.bgs.ac.uk/data_service/models_compass/coord_calc.html].

The work was financially supported by the Russian Science Foundation (Project No. 20-72-10170-P).

REFERENCES

Abunina M.A., Belov A.V., Eroshenko E.A., et al. Ring of station method in research of cosmic ray variations: 1. General description. *Geomagnetism and Aeronomy*. 2020, vol. 60, no. 1, pp. 38–45. DOI: 10.1134/S0016793220010028.

Alken P., Thébault E., Beggan C.D., et al. International geomagnetic reference field: The thirteenth generation. *Earth, Planets and Space*. 2021, vol. 73, pp. 1–25. DOI: 10.1186/s40623-020-01288-x.

Boris J.P. The acceleration calculation from a scalar potential. *Technical report MATT-152*. Princeton: Princeton University, 1970, 30 p.

Boris J.P. Relativistic plasma simulation — optimization of a hybrid code. *Proc. 4th Conf. on Numerical Simulation of Plasmas*. Washington, 1971, p. 3.

Cooke D.J., Humble J.E., Shea M.A., et al. On cosmic-ray cutoff terminology. *Nuovo Cimento C*. 1991, vol. 14, pp. 213–234. DOI: 10.1007/BF02509357.

Gerontidou M., Katzourakis N., Mavromichalaki H., et al. World grid of cosmic ray vertical cut-off rigidity for the last decade. *Adv. Space Res*. 2021, vol. 67, no. 7, pp. 2231–2240. DOI: 10.1016/j.asr.2021.01.011.

Gvozdevsky B., Belov A., Gushchina R., et al. Long-term changes in vertical geomagnetic cutoff rigidities of cosmic rays. *Physics of Atomic Nuclei*. 2018, vol. 81, pp. 1382–1389. DOI: 10.1134/S1063778818090132.

Mao H., Wirz R.E. Comparison of charged particle tracking methods for non-uniform magnetic fields. *42nd AIAA Plasmadynamics and Lasers Conference in conjunction with the 18th International Conference on MHD Energy Conversion (ICMHD)*. Honolulu, Hawaii, 2011, 9 p. DOI: 10.2514/6.2011-3739.

Mishev A.L., Koldobskiy S.A., Kovaltsov G.A., et al. Updated neutron-monitor yield function: Bridging between in situ and ground-based cosmic ray measurements. *J. Geophys. Res.: Space Phys*. 2020, vol. 125, no. 2, e27433. DOI: 10.1029/2019JA027433.

Poluianov S., Batalla O. Cosmic-ray atmospheric cutoff energies of polar neutron monitors. *Adv. Space Res*. 2022, vol. 70, no. 9, pp. 2610–2617. DOI: 10.1016/j.asr.2022.03.037.

Qin R., Zhang S., Xiao J., et al. Why is Boris algorithm so good? *Physics of Plasmas*. 2013, vol. 20, no. 8, 084503. DOI: 10.1063/1.4818428.

Smart D.F., Shea M.A. Vertical geomagnetic cut off rigidities for epoch 2015. *PoS 36th ICRC*. Madison, WI, USA, 2019, 1154.

Tezari A., Paschalis P., Mavromichalaki H., et al. Assessing radiation exposure inside the Earth's atmosphere.*Radiation Protection Dosimetry*. 2020, vol. 190, iss. 4, pp. 427–436. DOI: 10.1093/rpd/ncaa112.

Tyasto M.I., Danilova O.A., Ptitsyna N.G., Sdobnov V.E. Variations in cosmic ray cutoff rigidities during the great geomagnetic storm of November 2004. *Adv. Space Res*. 2013, vol. 51, no. 7, pp. 1230–1237. DOI: 10.1016/j.asr.2012.10.025.

URL: https://github.com/agmayorov/GTsimulation (accessed April 15, 2025).

URL: https://www.ncei.noaa.gov/products/international-geomagnetic-reference-field (accessed April 15, 2025).

URL: https://tools.izmiran.ru/cutoff / (accessed April 15, 2025).

URL: https://geomag.bgs.ac.uk/data_service/models_compass/coord_calc.html (accessed April 15, 2025).

Original Russian version: Kruchinin P.A., Siruk S.A., Mayorov A.G., Malakhov V.V., Aleksandrin S.Yu., published in Solnechno-zemnaya fizika. 2025, vol. 11, no. 2, pp. 132–138. DOI: 10.12737/szf-112202512.

How to cite this article

Kruchinin P.A., Siruk S.A., Mayorov A.G., Malakhov V.V., Aleksandrin S.Yu. Geomagnetic cutoff rigidity in neutron monitor locations. *Sol.-Terr. Phys*. 2025, vol. 11, iss. 2, pp. 119–124. DOI: 10.12737/stp-112202512.